

The role of silanol nests in the activation of the $[\text{Fe}=\text{O}]^{2+}$ group in the reaction of hydrogen atom transfer from methane.

V.Yu. Kovalskii¹

¹Boreshkov Institute of Catalysis SB RAS, Lavrentieva ave. 5, Novosibirsk, Russia, 630090

Abstract

Silanol nests can play the role of places into which positively charged groups, such as, $[\text{FeO}]^{2+}$, can invade. In the framework of this work, the influence of such structures on the activity of the $[\text{FeO}]^{2+}$ group in the reaction of detachment of a hydrogen atom from methane was considered. Two ways of the reaction of hydrogen atom transfer (HAT) from methane were found: the so-called ferryl and oxyl routes. It was shown that the reaction of the detachment of a hydrogen atom from methane, which is a limiting stage of the oxidation of methane to methanol at the alpha center, proceeds through the formation of the so-called oxidation state $[\text{Fe}(\text{III})-\text{O}(-)]^{2+}$, and fingerprint of this state is negative spin density on oxo moiety.

Introduction

The methane binding problem is one of the most difficult problems, since methane oxidation requires breaking or at least weakening the C-H bond, whose energy is about 140 kcal/mol. Some living organisms are able to absorb methane from the gas phase due to the presence of enzymes that can bind methane under mild conditions, such as methane monooxygenase. The complexity of using enzymes in industry is that it is difficult to organize large-tonnage production. It is known that a large number of these enzymes contains the group $[\text{M}=\text{O}]$ with active oxygen, on which the partial oxidation of methane takes place. Based on information on the structure of these enzymes, a large number of biomimetic catalysts were synthesized and tested, but they are all inferior in oxidizing ability to enzymes and are also difficult to use in large-tonnage production, as are enzymes.

To solve this problem, there were attempts to create systems containing $[\text{M}=\text{O}]$ based on, among other things, zeolites. One of the successful examples of this approach can be considered the so-called Panov alpha-oxygen, capable of oxidizing methane and benzene under mild conditions with a fairly high [1,2]. Despite a fairly lengthy study of this system, the structure of the active center has not yet been uniquely determined. The active center model in the form of the monomer $[\text{Fe}=\text{O}]^{2+}$ with a bond length of about 1.6 Å localized in the cation exchange position of the zeolite lattice predominates.[3] In some works, it is represented as an iron dimer, but only one oxygen atom acts as an active fragment. [4] The literature also mentions the possibility of the formation of iron trimers in the structure of Fe-ZSM-5, similar to the structure of the active center of ferredoxin II, Fe_3S_4 . [5] In the literature, most often the group containing iron is placed in a six-membered ring, as the most likely place for the introduction of such a structure. In addition to such places, there are so-called "hydroxyl nests" (hydroxyl or silanol nests). "Hydroxyl nests" are formed during dealumination of the initial zeolite, as a result of which tetrahedral aluminum is removed from the zeolite framework.

So, for example, when processing in solutions of inorganic acids at a pH of less than 4, the structure of zeolite Y is destroyed, while at a pH of more than 4, partial amorphization and simultaneous dealumination of the zeolite framework occurs. In this case, 2 reactions proceed sequentially: decationation and dealumination due to the formation of the Brønsted acid center (BCC).

Aluminum in the BCC is weaker bound to the framework and leaves it.[6] In this case, a structural defect is formed - the “hydroxyl nest”, consisting of four hydroxyl groups. (Figure 1)

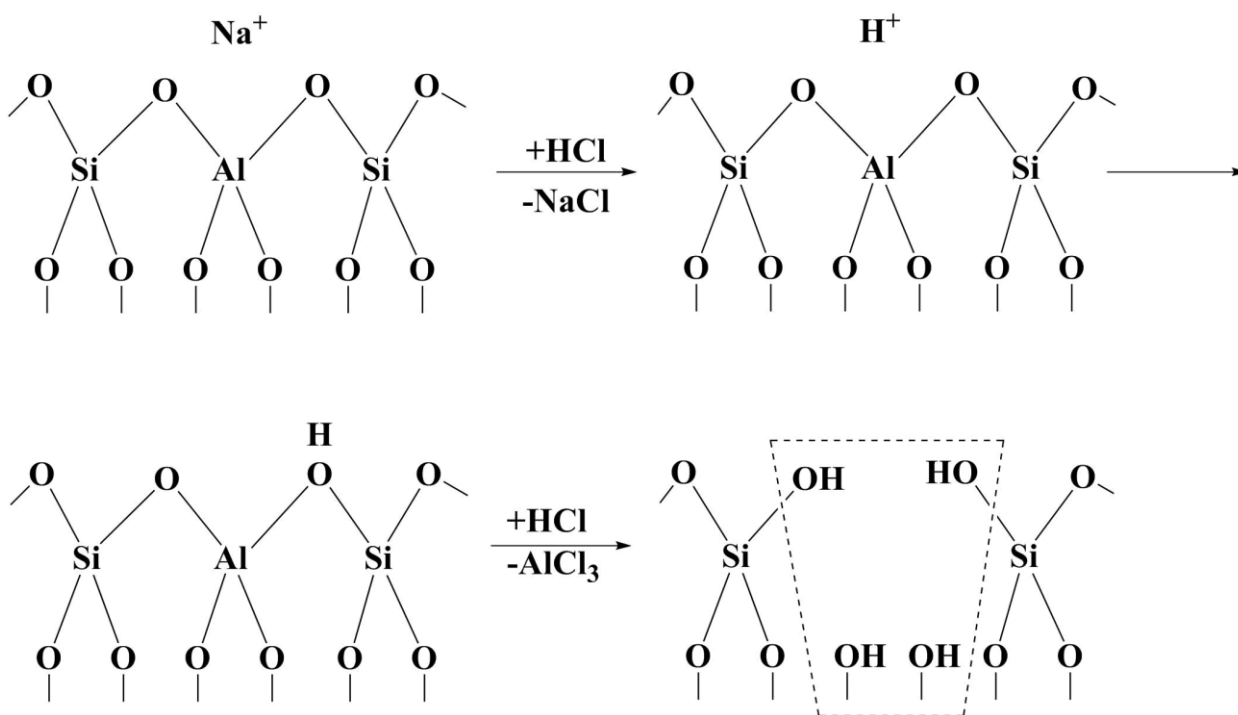


Figure 1. The scheme of formation of the "hydroxyl nest", consisting of four hydroxyl groups.

“Hydroxyl nests” can play the role of places into which positively charged groups, such as, $[\text{FeO}]^{2+}$, can invade. In the framework of this work, the influence of such structures on the activity of the $[\text{FeO}]^{2+}$ group in the reaction of detachment of a hydrogen atom from methane was considered. Earlier in our works, using the example $\text{O}=\text{Fe}(\text{OH})_2$, two ways of the reaction of the detachment of a hydrogen atom from methane were found: the so-called ferryl (generally, amyl) and oxyl routes. It was shown that the reaction of the detachment of a hydrogen atom from methane, which is a limiting stage of the oxidation of methane to methanol at the alpha center, proceeds through the formation of the so-called oxidation state $[\text{Fe}---\text{O}^*]^{2+}$, and fingerprint of this state is negative spin density on oxo moiety.[7] It should be noted that in many studies, the oxidized state refers to the $\text{Fe}-\text{O}$ group with an elongated bond (up to 1.7–1.8 Å) and an oxygen center with some positive spin density, which is interpreted as evidence of the radical nature of this center. [8] However, in specific calculations, both in the ferryl and in the oxyl state, there is a noticeable magnitude of spin density, positive and negative signs, respectively.[?] A negative spin density oxo center was first identified by Morokuma [9]. Morokuma et al., When considering the reaction of the detachment of a hydrogen atom from methane in a methane monooxygenase model, found that in the transition state a negative spin density appears on the terminal oxygen atom and a methyl radical with a negative spin density forms. The authors associated the appearance of negative spin density on the methyl radical with the fact that two iron atoms are ferromagnetically coupled; therefore, the methyl radical must bind antiferromagnetically in order to satisfy the total spin moment of 9.

Baerends investigated the active center models of the alpha center containing $[\text{FeO}]^{2+}$ in the form $\text{O}=\text{M}(\text{H}_2\text{O})_5^{2+}$ by DFT [10] and by Car-Parinello method [11]. To explain the appearance of negative spin density on the methyl radical, the authors proposed a mechanism involving the transfer of α electron from methane to σ^* the iron orbital. Thus, five unpaired α electrons are formed on the iron atom, and the β electron remains on the methyl radical. Baerends et al suggested that the activity of the $[\text{M}=\text{O}]^{2+}$ group correlates with the position of the first unoccupied orbital

(σ^*). The lower the energy of this orbital, the higher the activity, estimated by the magnitude of the hydrogen separation barrier.

But this mechanism has several disadvantages. So, for example, he cannot explain the oxidative nature of the transition state, which is noted in many computational works [8,12] in which the unoccupied orbital σ^* is filled with its own electron and becomes inaccessible to the hydrogen electron. But this mechanism does not explain the appearance of negative spin density on oxygen during the reaction in the early stages.

Nesse in his work [8] proposes such a mechanism: oxidative oxygen is more active than oxoligand and has a higher electrophilicity. Thus, it is possible to imagine the activation of the C – H bond as a process consisting of a preparatory stage, at which the curve intersects between the ground state of $[\text{FeO}]^{2+}$ and the state of charge transfer from the ligand to the metal, followed by the stage of detachment of the hydrogen atom. As explained by PCET theory [doi:10.1146/annurev.physchem.49.1.337], the latter can proceed as proton transfer followed by electron transfer, vice versa or simultaneously. The activity of $[\text{FeO}]^{2+}$ Neese associates with the fact that, at the preparatory stage, the ability of $[\text{FeO}]^{2+}$ to interact with the CH binding orbital is enhanced, since the O- p_z orbital overlaps with the CH σ bond more efficiently than the Fe- d_{z^2} antibonding orbital, which includes only the limited nature of O- p_z . Enhanced overlap greatly facilitates electron transfer and the formation of three-center MOs observed in the transition state. The oxyl-oxygen is intrinsically much more reactive than the oxo-ligand and is highly electrophilic. Thus, one may picture the C–H bond activation process as consisting of a preparatory step in which there is a curve crossing between the ground state of the $(\text{FeO})^{2+}$ core and a LMCT (Ligand-to-metal (ion) charge transfer) state, followed by the genuine C–H abstraction step. The preparatory step greatly enhances the ability of the $(\text{FeO})^{2+}$ core to interact with the bonding C–H s-orbital since the O- p_z orbital more efficiently overlaps with the C–Hs-bond than the Fe- d_{z^2} antibonding orbital that only involves limited O- p_z character. The enhanced overlap greatly facilitates electron transfer and formation of the three-center MOs observed in transition state.

Solomon: [13]

The mechanism for activating the iron–oxo intermediate for electrophilic reactivity is the same for both, aromatic electrophilic attack and hydrogen-atom abstraction: Elongation of the Fe-O bond transforms the ferryl-oxo, $\text{Fe}^{\text{IV}}=\text{O}^{2-}$, to a ferric-oxyl, $\text{Fe}^{\text{III}}-\text{O}^\bullet$ species in the transition state. The short Fe-O bond in the $\text{Fe}^{\text{IV}}=\text{O}$ intermediate allows for large σ - and especially π -overlap between the iron d- and oxo p-orbitals, forming a strong covalent bond, which enables significant charge donation from the oxo to the iron to stabilize the high oxidation state. Elongation of the Fe-O bond decreases the overlap and significantly reduces the charge donation. In this case, one electron is transferred from the oxo to the iron, which results in significant spin polarization and the bi-radical character of the ferric-oxyl transition state. The dominant radical character on the oxygen significantly increases its electrophilicity, enhancing the reactivity with the electron density on the aromatic π -system or the C-H σ -bond.

In the transition state for hydrogen-atom abstraction, energy is required to partially break the C-H bond. Thus, this activation energy is somewhat dependent on the C-H bond strength of the substrate.

Earlier, we studied systems containing the $[\text{Fe}=\text{O}]^{2+}$: monomer $\text{O}=\text{Fe}(\text{OH})_2$, dimer $\text{OFe}_2(\text{OH})_5$ and tetramer $\text{OFe}_4(\mu\text{-O})_4(\text{OH})_3$. When simulating the first stage of C-H bond C-H:

$[\text{Fe}=\text{O}]^{2+} + \text{CH}_4 \rightarrow [\text{FeOH}]^{2+} + \text{CH}_3^\bullet$ two reaction routes, the so-called oxyl and ferryl routes, were detected.

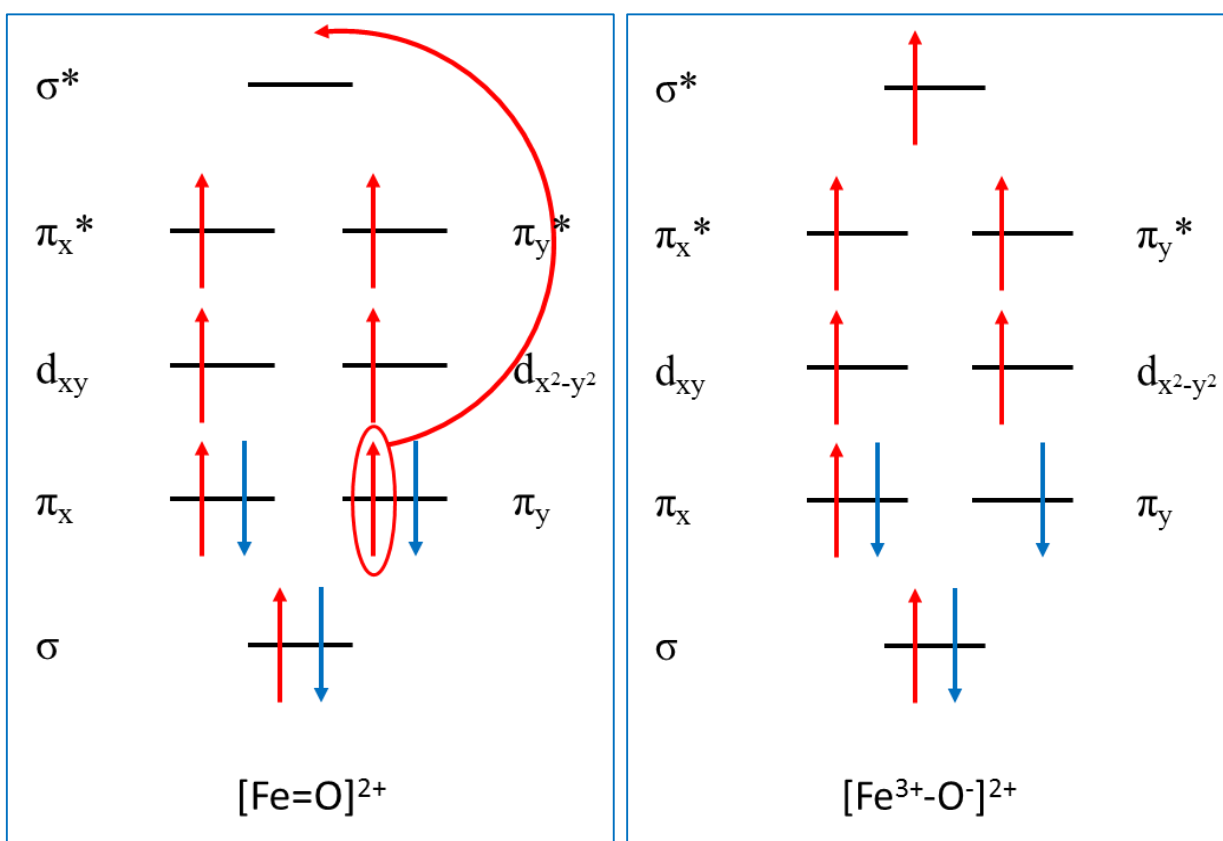
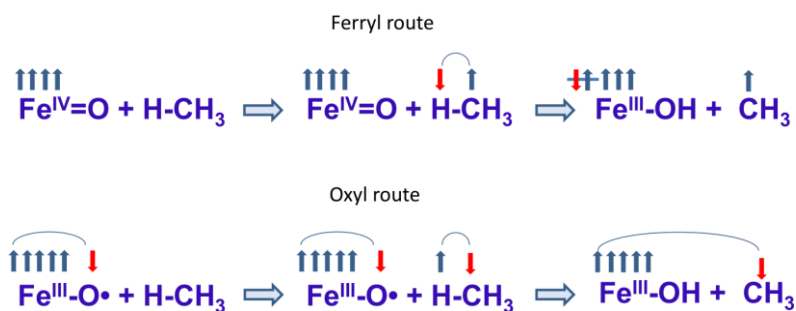


Figure 2. Scheme of formation oxyl state $[\text{Fe}^{3+}-\text{O}]^{2+}$ from ferryl state $[\text{Fe}=\text{O}]^{2+}$.

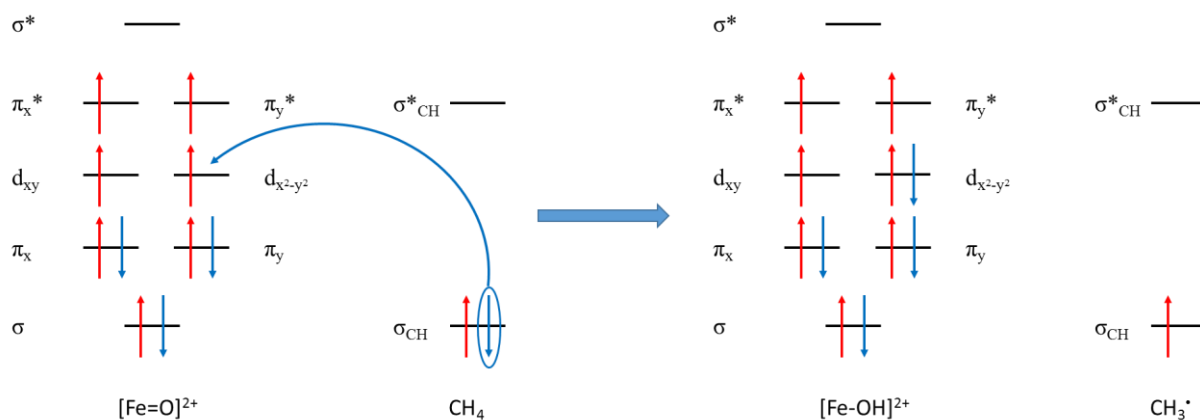


Figure 3. Ferryl route $[FeO]^{2+} + CH_4$.

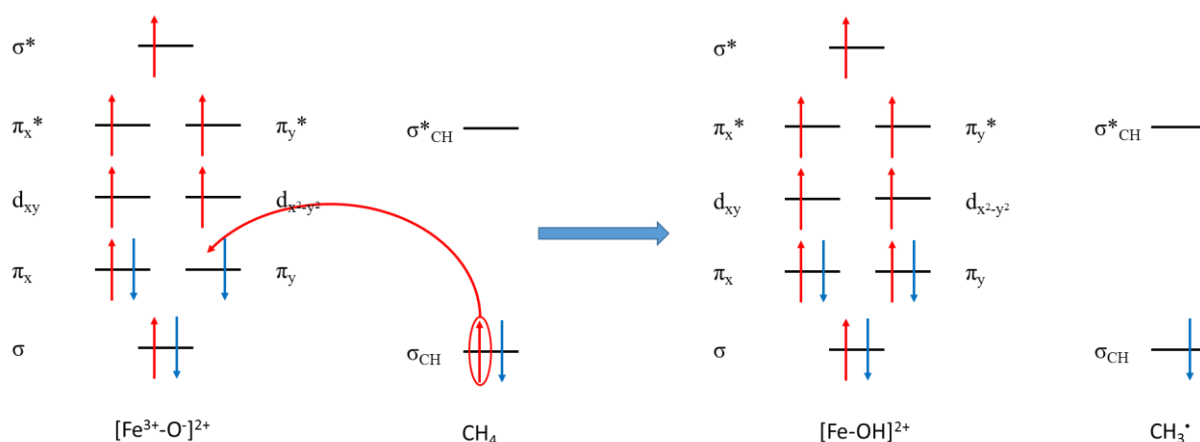


Figure 4. Oxyl route $[FeO]^{2+} + CH_4$.

In reality, the reaction from the hydrogen atom proceeds through the oxyl state Figure 2. Then the reaction proceeds in the oxide stream in accordance with the instructions, Figure 4. The ferryl path can be realized, but the barrier reaction is due to higher than in the oxyl scenario. [14]

In this paper, we solve the problem of studying the possible effect of structures on the similarity of “hydroxyl nests” on the state and reactivity of the oxo center of the ferryl group in simple models containing Al and Ga atoms. Various model structures of the Fe-ZSM-5 cluster from simple to more complex are considered: $O=Fe(OM(OH)_2)_2$, $O=Fe(M(OH)_2)_2(\mu-O)_4(Si(OH)_2)_2$ и 6-ring model ZSM-5 (FeM2Si5H12O21). The first one ($O=Fe(OM(OH)_2)_2$) were formed by changing hydrogen atom at $O=Fe(OH)_2$ by $M(OH)_2^+$, where $M=Al, Ga$. Thus, we can try to take into account the influence of the ligand environment in a rather simple approximation. The second model, $O=Fe(M(OH)_2)_2(\mu-O)_4(Si(OH)_2)_2$, was formed by forming a cation-exchange position in a four-membered silicon cycle. The latter model was formed on the basis of the model of the active center FeZSM-5, in which the model is simplified to the maximum to facilitate the calculation, but at the same time retaining the active zeolite ring. [15].

ZSM-5 Models

$O=Fe(OM(OH)_2)$, $M=Al, Ga$.

To determine the effect of the ligand environment on the $[FeO]^{2+}$ activity, the previously studied model particle of α -oxygen $O=Fe(OH)_2$ was taken and the hydrogen atom in it was replaced by the group $M(OH)_2$, where $M=Al, Ga$. This group has the same symmetry as $O=Fe(OH)_2$;

thus, it is possible to evaluate the effect of the ligand environment on the stabilization of the oxide state and the change in the separation barrier of the hydrogen atom from methane.

Al

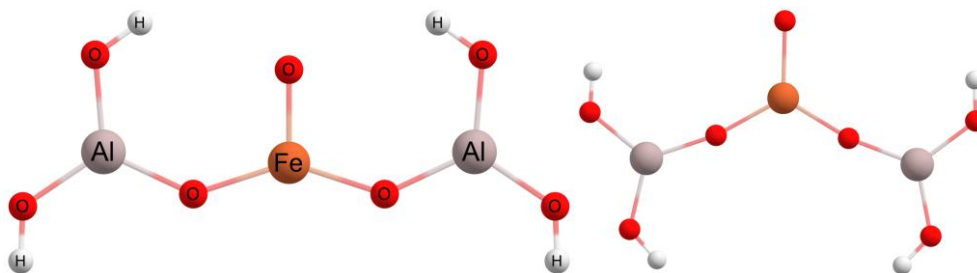


Figure 5. The $O=Fe(OAl(OH)_2)$ model: 5A_1 and 5B_1 states.

In a previously published article [16] for the $O=Fe(OH)_2$ system the authors showed that the 5B_1 и 5B_2 oxyl state is higher in energy relative to the 5A_1 ground state by 42 and 21 kcal/mol, respectively, and 5A_2 – by 51 kcal/mol. For our model, 5A_2 is also by 53 kcal/mol, and the 5B_1 и 5B_2 oxyl states are 20 и 10.5 kcal/mol higher, which is significantly lower than for $O=Fe(OH)_2$ (Table 1). That is, even in such a simple model, the influence of the ligand environment on the stabilization of the oxide state is significant.

CH_4 oxidation

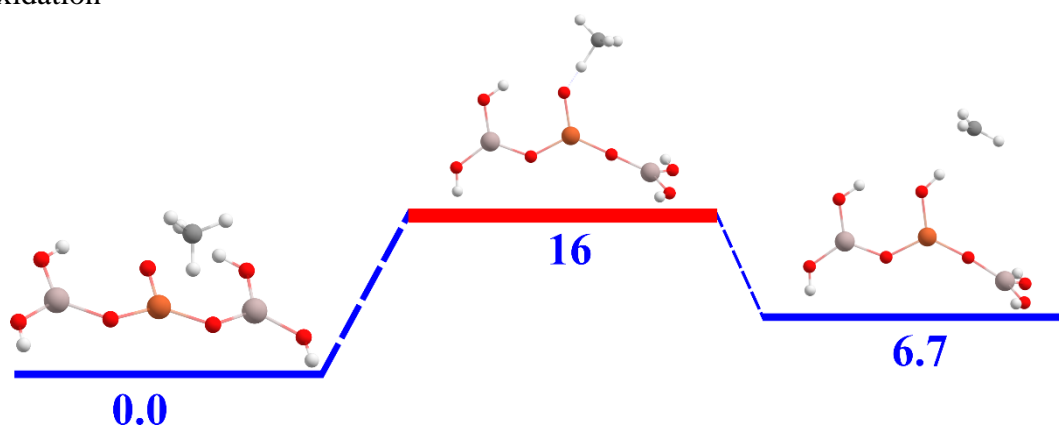


Figure 6. Reaction path $O=Fe(OAl(OH)_2)+CH_4$. Energies in kcal/mol relative to reactants.

Despite the stabilization of the oxide state, the hydrogen atom detachment barrier, 16 kcal/mol (Table 2), does not differ much from the previously published value for the oxyl – 18 kcal/mol [14]. The reaction proceeds through an oxide transition state, the hallmark of which is the emerging negative spin density on the methyl, $q_s(C) = -0.490$ (Table 2). The angle $\angle(O-Fe-C)$ is about 130 degrees, which corresponds to a π -attack, as previously indicated in an article by Shaik et al. [17] The authors argue that at $S_z=2$ the angle of attack of approximately 120° should correspond to the formation of a methyl radical with α -spin, that is, with a positive spin density. In our calculations, when the angle of attack is 130° , which corresponds to a π -attack, a negative spin density is formed on the methyl radical in the intermediate. Therefore, we suggested that the mechanism proposed by Shaik is not correct.

Ga

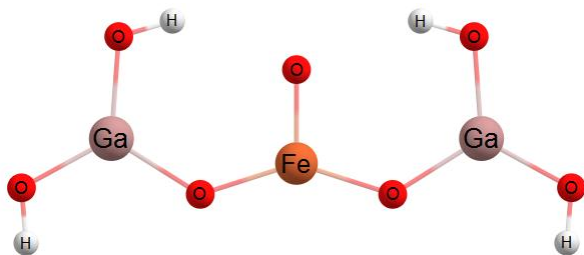


Figure 7. The $O=Fe(OGa(OH)_2)$ model: NoSymm state.

CH_4 oxidation

When Al is replaced by Ga, the separation barrier of the hydrogen atom from methane by $O=Fe(OGa(OH)_2)$ practically doesn't change and is equal to 18 kcal/mol. Thus, we can conclude that the direct influence of the metal on the course of the reaction is practically absent.

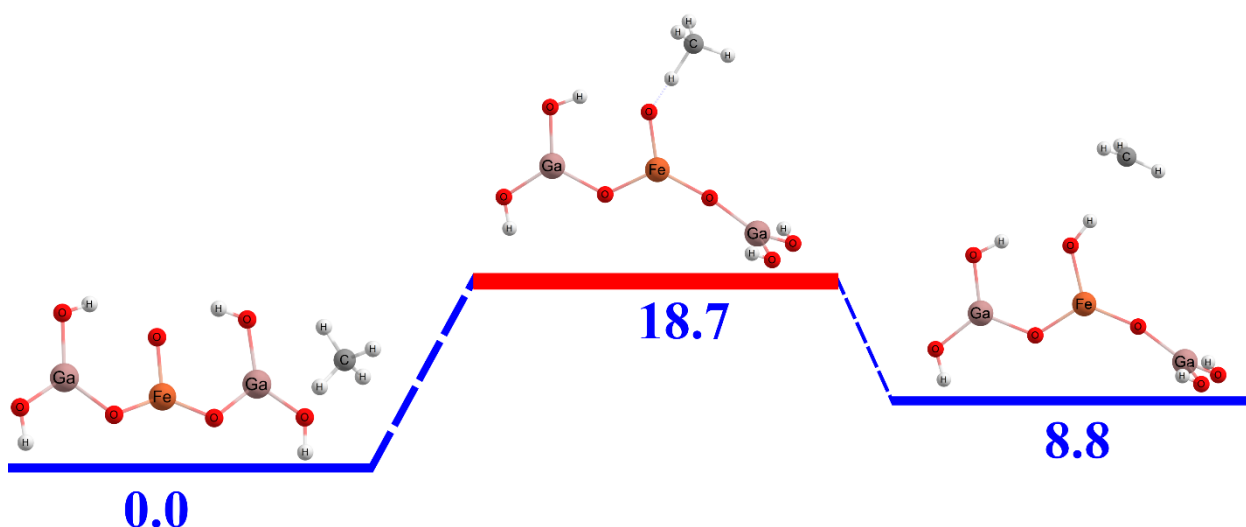


Figure 8. . Reaction path $O=Fe(OGa(OH)_2)+CH_4$. Energies in kcal/mol relative to reactants.

$O=Fe(M(OH)_2)_2(\mu-O)_4(Si(OH)_2)_2$, $M=Al, Ga$.

Al

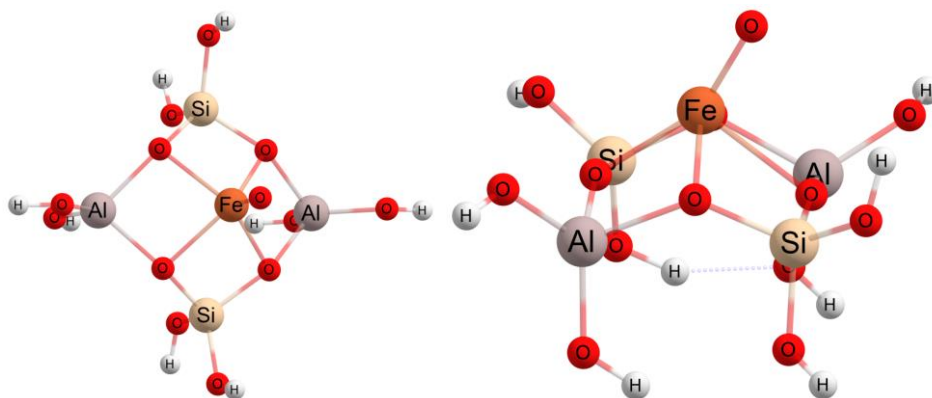


Figure 9. $O=Fe(M(OH)_2)_2(\mu-O)_4(Si(OH)_2)_2$ Model: 5A_1 and NoSymm structure.

When using the four-membered cycle, it is possible to significantly stabilize the oxyl states (5B_1 and 5B_2); they are comparable in energy to 5A_1 (Table 5). When symmetry is disabled (NoSymm structure), the energy of the system drops by 9.4 kcal / mol (Table 5). Therefore, we can assume that a system with artificially specified symmetry is a stressed structure. Under certain circumstances, if the environment can create such a tense structure, the oxidation state can become

the ground state. One of such circumstances may be a geometric factor, and specifically $\angle(\text{O-Fe-O})$, as it was previously shown that the influence of this angle on the stabilization of the oxidation state is significant. [18] So for the oxyl state is characterized by lower values of the angle $\angle(\text{O-Fe-O})$.

CH_4 oxidation

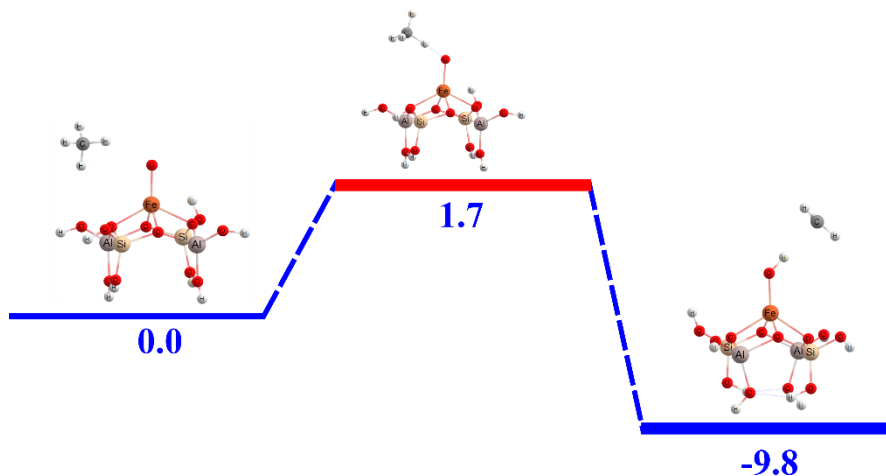


Figure 10. Reaction path $\text{O}=\text{Fe}(\text{Al}(\text{OH})_2)_2(\mu\text{-O})_4(\text{Si}(\text{OH})_2)_2+\text{CH}_4$. Energies in kcal/mol relative to reactants.

For a structure with a four-membered ring, the hydrogen atom detachment reaction barrier is only 1.7 kcal/mol. Therefore, for structures like these, a very high activity in the HAT reaction can be expected. Такие структуры могут образоваться в процессах формирования ранее упомянутых «гидроксильных гнезд».

Ga

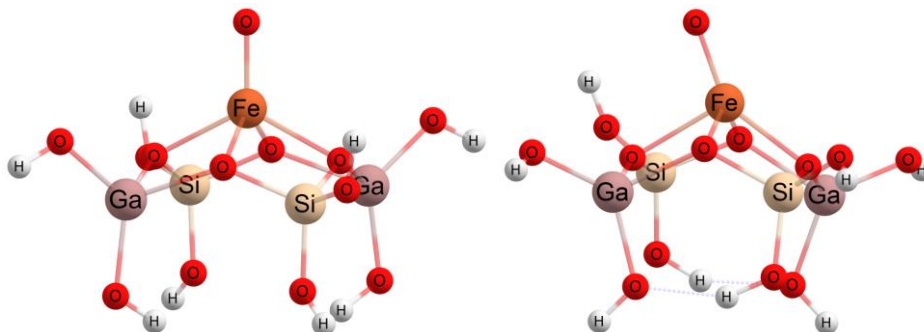


Figure 11. The $\text{O}=\text{Fe}(\text{M}(\text{OH})_2)_2(\mu\text{-O})_4(\text{Si}(\text{OH})_2)_2$ model: ${}^5\text{A}_1$ and NoSymm structure.

CH₄ oxidation

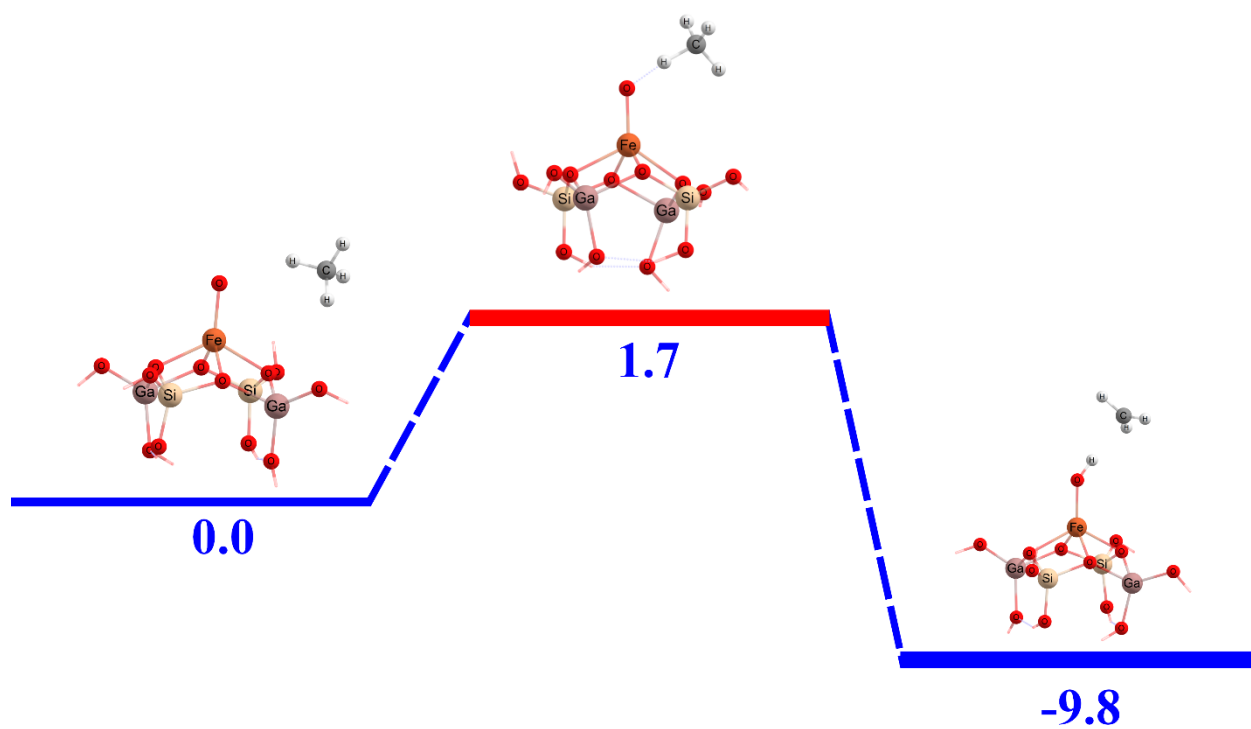


Figure 12. Reaction path $O=Fe(Ga(OH)_2)_2(\mu-O)_4(Si(OH)_2)_2+CH_4$. Energies in kcal/mol relative to reactants.

6-ring model ZSM-5 (FeM₂Si₅H₁₂O₂₁, M=Al, Ga.)

Al

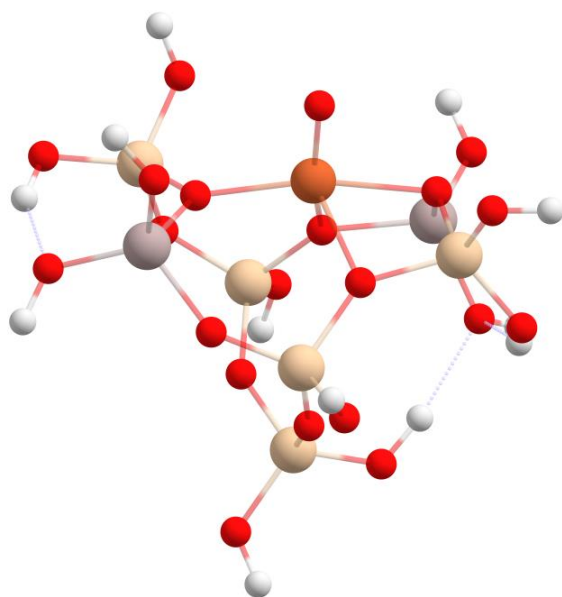


Figure 13. 6-ring model ZSM-5 (FeAl₂Si₅H₁₂O₂₁)

CH₄ oxidation

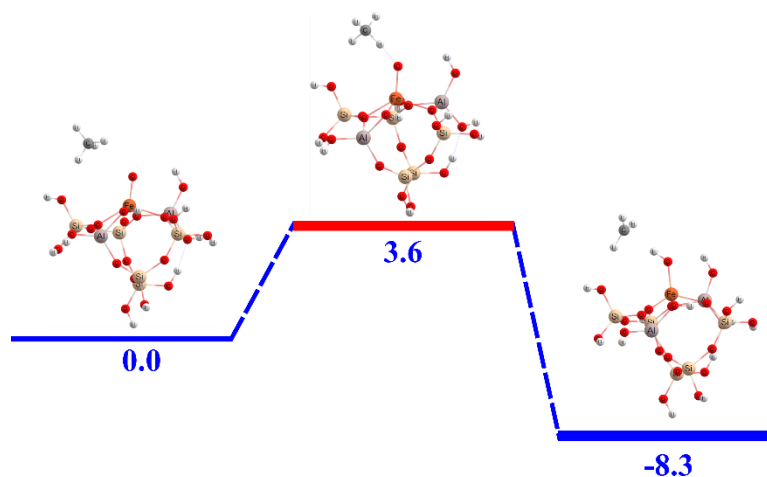


Figure 14. Reaction path $\text{FeAl}_2\text{Si}_5\text{H}_{12}\text{O}_{21} + \text{CH}_4$. Energies in kcal/mol relative to reactants.

Ga

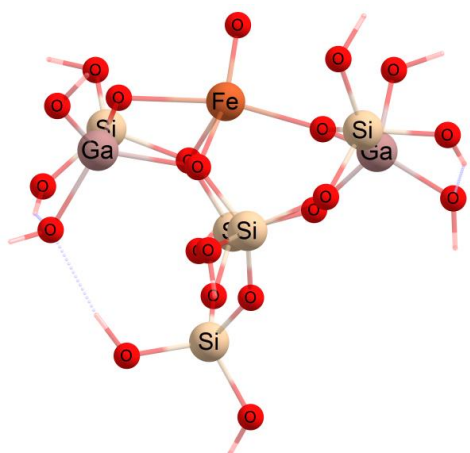


Figure 15. 6-ring model ZSM-5 ($\text{FeGa}_2\text{Si}_5\text{H}_{12}\text{O}_{21}$)

CH₄ oxidation

HAT on 6-ring model протекает с барьером, сопоставимым с ранее приведённым в литературе барьером для модели цеолита Fe-ZSM-5 [15] и для модели гидроксида железа в виде кубана $\text{O}=\text{Fe}_4(\mu\text{-O})_4(\text{OH})_3$ [7].

Discussion

Acknowledgments

The reported study was funded by RFBR according to the research project № [18-33-00932](#).

References

- [1] V.I. Sobolev, K.A. Dubkov, O. V. Panna, G.I. Panov, Selective oxidation of methane to methanol on a FeZSM-5 surface, *Catal. Today*. 24 (1995) 251–252. doi:10.1016/0920-5861(95)00035-E.
- [2] K.A. Dubkov, V.I. Sobolev, E.P. Talsi, M.A. Rodkin, N.H. Watkins, A.A. Shteinman, G.I.

- Panov, Kinetic isotope effects and mechanism of biomimetic oxidation of methane and benzene on FeZSM-5 zeolite, *J. Mol. Catal. A Chem.* 123 (1997) 155–161. doi:10.1016/S1381-1169(97)00051-4.
- [3] B.E.R. Snyder, P. Vanelderen, M.L. Bols, S.D. Hallaert, L.H. Böttger, L. Ungur, K. Pierloot, R.A. Schoonheydt, B.F. Sels, E.I. Solomon, The active site of low-temperature methane hydroxylation in iron-containing zeolites, *Nature*. 536 (2016) 317–321. doi:10.1038/nature19059.
- [4] K.A. Dubkov, N.S. Ovanesyan, A.A. Shteinman, E. V. Starokon, G.I. Panov, Evolution of iron states and formation of α -sites upon activation of FeZSM-5 zeolites, *J. Catal.* 207 (2002) 341–352. doi:10.1006/jcat.2002.3552.
- [5] R.W. Joyner, M. Stockenhuber, Unusual structure and stability of iron-oxygen nano-clusters in Fe-ZSM-5 catalysts, *Catal. Letters*. 45 (1997) 15–19. doi:10.1023/A:1019063511784.
- [6] Н.Н. Шавалеева, СИНТЕЗ И СВОЙСТВА ГРАНУЛИРОВАННЫХ УЛЬТРАСТАБИЛЬНЫХ ЦЕОЛИТОВ γ , НЕ СОДЕРЖАЩИХ СВЯЗУЮЩИХ ВЕЩЕСТВ, ФЕДЕРАЛЬНОЕ ГОСУДАРСТВЕННОЕ БЮДЖЕТНОЕ УЧРЕЖДЕНИЕ НАУКИ ИНСТИТУТ НЕФТЕХИМИИ И КАТАЛИЗА РОССИЙСКОЙ АКАДЕМИИ НАУК, 2016.
- [7] A.A. Shubin, S.P. Ruzankin, I.L. Zilberberg, V.N. Parmon, Distinct activity of the oxyl Fe III O group in the methane dissociation by activated iron hydroxide: DFT predictions, *Chem. Phys. Lett.* 640 (2015) 94–100. doi:10.1016/j.cplett.2015.10.016.
- [8] S. Ye, F. Neese, Quantum chemical studies of C-H activation reactions by high-valent nonheme iron centers, *Curr. Opin. Chem. Biol.* 13 (2009) 89–98. doi:10.1016/j.cbpa.2009.02.007.
- [9] H. Basch, K. Mogi, D.G. Musaev, K. Morokuma, Mechanism of the methane \rightarrow methanol conversion reaction catalyzed by methane monooxygenase: A density functional study, *J. Am. Chem. Soc.* 121 (1999) 7249–7256. doi:10.1021/ja9906296.
- [10] C. Michel, E.J. Baerends, What singles out the FeO₂+moiety? A density-functional theory study of the methane-to-methanol reaction catalyzed by the first row transition-metal oxide dications MO(H₂O)_p2+, M) V-Cu, *Inorg. Chem.* 48 (2009) 3628–3639. doi:10.1021/ic802095m.
- [11] B. Ensing, F. Buda, M.C.M. Gribnau, E.J. Baerends, Methane-to-Methanol Oxidation by the Hydrated Iron(IV) Oxo Species in Aqueous Solution: A Combined DFT and Car-Parrinello Molecular Dynamics Study, *J. Am. Chem. Soc.* 126 (2004) 4355–4365. doi:10.1021/ja038865a.
- [12] W. Lai, C. Li, H. Chen, S. Shaik, Hydrogen-abstraction reactivity patterns from A to Y: The valence bond way, *Angew. Chemie - Int. Ed.* 51 (2012) 5556–5578. doi:10.1002/anie.201108398.
- [13] M.L. Neidig, A. Decker, O.W. Choroba, F. Huang, M. Kavana, G.R. Moran, J.B. Spencer, E.I. Solomon, Spectroscopic and electronic structure studies of aromatic electrophilic attack and hydrogen-atom abstraction by non-heme iron enzymes, *Proc. Natl. Acad. Sci.* 103 (2006) 12966–12973. doi:10.1073/pnas.0605067103.
- [14] V. Kovalskii, A. Shubin, Y. Chen, D. Ovchinnikov, S.P. Ruzankin, J. Hasegawa, I. Zilberberg, V.N. Parmon, Hidden radical reactivity of the [FeO]₂+group in the H-abstraction from methane: DFT and CASPT2 supported mechanism by the example of

- model iron (hydro)oxide species, Chem. Phys. Lett. 679 (2017) 193–199.
doi:10.1016/j.cplett.2017.05.002.
- [15] A. Rosa, G. Ricciardi, E.J. Baerends, Is [FeO]²⁺ the Active Center Also in Iron Containing Zeolites? A Density Functional Theory Study of Methane Hydroxylation Catalysis by Fe-ZSM-5 Zeolite, Inorg. Chem. 49 (2010) 3866–3880.
doi:10.1021/ic1000073.
- [16] I. Zilberberg, R.W. Gora, G.M. Zhidomirov, J. Leszczynski, Bonding in the oxo ferrous iron species: A complete active-space self-consistent-field theory verification of the molecular-oxygen-like pattern, J. Chem. Phys. 117 (2002) 7153–7161.
doi:10.1063/1.1506913.
- [17] S. Shaik, H. Chen, D. Janardanan, Exchange-enhanced reactivity in bond activation by metal–oxo enzymes and synthetic reagents, Nat. Chem. 3 (2011) 19–27.
doi:10.1038/nchem.943.
- [18] S. Malykhin, I. Zilberberg, G.M. Zhidomirov, Electron structure of oxygen complexes of ferrous ion center, Chem. Phys. Lett. 414 (2005) 434–437.
doi:10.1016/j.cplett.2005.08.101.
- [19] M.J. Frisch, G.W. Trucks, H.B. Schlegel, G.E. Scuseria, M.A. Robb, J.R. Cheeseman, G. Scalmani, V. Barone, B. Mennucci, G.A. Petersson, H. Nakatsuji, M. Caricato, X. Li, H.P. Hratchian, A.F. Izmaylov, J. Bloino, G. Zheng, J.L. Sonnenberg, M. Hada, M. Ehara, K. Toyota, R. Fukuda, J. Hasegawa, M. Ishida, T. Nakajima, Y. Honda, O. Kitao, H. Nakai, T. Vreven, J.A. Montgomery Jr., J.E. Peralta, F. Ogliaro, M. Bearpark, J.J. Heyd, E. Brothers, K.N. Kudin, V.N. Staroverov, R. Kobayashi, J. Normand, K. Raghavachari, A. Rendell, J.C. Burant, S.S. Iyengar, J. Tomasi, M. Cossi, N. Rega, J.M. Millam, M. Klene, J.E. Knox, J.B. Cross, V. Bakken, C. Adamo, J. Jaramillo, R. Gomperts, R.E. Stratmann, O. Yazyev, A.J. Austin, R. Cammi, C. Pomelli, J.W. Ochterski, R.L. Martin, K. Morokuma, V.G. Zakrzewski, G.A. Voth, P. Salvador, J.J. Dannenberg, S. Dapprich, A.D. Daniels, Ö. Farkas, J.B. Foresman, J. V Ortiz, J. Cioslowski, D.J. Fox, Gaussian~09 {R}evision {D}.01, (n.d.).
- [20] A.D. Becke, Density-functional thermochemistry. III. The role of exact exchange, J. Chem. Phys. 98 (1993) 5648–5652. doi:10.1063/1.464913.
- [21] C. Lee, W. Yang, R.G. Parr, Development of the Colle-Salvetti correlation-energy formula into a functional of the electron density, Phys. Rev. B. 37 (1988) 785–789.
doi:10.1103/PhysRevB.37.785.

Supporting materials

Computational details

All calculations were performed using by Gaussian'09 package [19] on UB3LYP/6-311++G(d,p) level. [20,21] All systems were uncharged and in quintet state ($S_z=2$).

SCF=(tight,Conver=8) int=(grid=UltraFine)

Charge = 0 Multiplicity = 5.

Table 1. The different states of $O=Fe(OAl(OH)_2)_2$ model in C_{2v} point group: energy, geometrical parameters, spin densities, $\langle S^2 \rangle$ and energy of 1s-orbital of Fe and O from group $[FeO]^{2+}$.

Symmetry	⁵ A ₁	⁵ A ₂	⁵ B ₁	⁵ B ₂	NoSymm
----------	-----------------------------	-----------------------------	-----------------------------	-----------------------------	--------

Energy, a.u.	-2278.12981301	-2278.04541890	-2278.09727860	-2278.11304619	-2278.12981432
E _{rel} , kcal/mol	0	52.95892781	20.41647339	10.52216087	0
d(Fe=O), Å	1.62553	1.73739	1.80953	1.71269	1.62562
∠(O-Fe=O)	108.124	110.540	120.278	122.753	108.115
∠(O-Fe-O)	143.752	138.920	119.444	114.493	143.768
<S ² >	6.0596	6.5835	6.8115	6.5558	6.0596
q _s (Fe)	3.176	3.641	4.133	3.897	3.176
q _s (O)	0.544	0.983	-0.688	-0.399	0.544
E(Fe1s), a.u.	-256.193568	-256.161139	-256.197110	-256.195859	-256.193620
E(O1s), a.u.	-19.172867	-19.129572	-19.166425	-19.173770	-19.172910
E(Fe1s), eV	-6971,382075	-6970,499637	-6971,478457	-6971,444416	-6971,38349
E(O1s), eV	-521,720285	-520,5421681	-521,5449893	-521,7448569	-521,7214551
E _{rel} (Fe1s), eV	0	0,882438	-0,096382	-0,062341	-0,001415
E _{rel} (O1s), eV	0	1,1781169	0,1752957	-0,0245719	-0,0011701

$$E_{\text{ads}} = E(\text{NoSymm}+\text{CH}_4) - (E(\text{NoSymm}) + E(\text{CH}_4)) = -2318.66454894 - (-2278.12981432 - 40.5339575449) = -0,000777075 \text{ (a.u.)} = -0,487622007 \text{ (kcal/mol)}$$

Table 2. Characteristics of adsorbed system, reactants, transition state and products for $\text{O}=\text{Fe}(\text{OAl}(\text{OH})_2)+\text{CH}_4$.

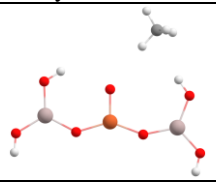
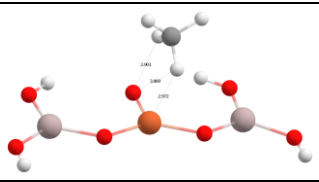
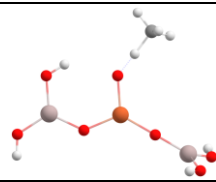
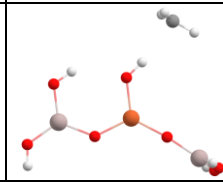
Structure	NoSymm+CH ₄	Reactants	TS	Products
				
Energy, a.u.	-2318.66454894	-2318.66454600	-2318.63879039	-2318.65391320
E _{rel} , kcal/mol	0	0,001844878	16,16373483	6,67402789
d(Fe=O), Å	1.62442	1.62676	1.75919	1.82181
∠(O-Fe=O)	106.763	108.071	108.858	110.151
∠(O-Fe-O)	142.431	143.376	127.478	125.614
∠(Fe-O-H)	143.24	72.025	137.805	128.115
∠(Fe-O-C)	141.660	62.068	138.431	134.307
<S ² >	6.0607	6.0601	6.7128	7.0050
q _s (Fe)	3.184	3.180	3.999	4.145
q _s (O)	0.540	0.539	-0.034	0.294
q _s (H)	0	0.001	0.015	-0.029
q _s (C)	-0.001	0.006	-0.490	-1.075
E(Fe1s), a.u.	-256.192350	-256.191130	-256.176520	-256.176540
E(O1s), a.u.	-19.171040	-19.170210	-19.147460	-19.135720
E(Fe1s), eV.	-6971,348931	-6971,315733	-6970,918175	-6970,918719
E(O1s), eV	-521,6705698	-521,6479844	-521,0289254	-520,7094637
E _{rel} (Fe1s), eV	0	0,033198	0,430756	0,430212
E _{rel} (O1s), eV	0	0,0225854	0,6416444	0,9611061

Table 3. The different states of $\text{O}=\text{Fe}(\text{OGa}(\text{OH})_2)_2$ model in C_{2v} point group: energy, geometrical parameters, spin densities, <S²> and energy of 1s-orbital of Fe and O from group [FeO]²⁺.

Symmetry	⁵ A ₁	⁵ A ₂	⁵ B ₁	⁵ B ₂	NoSymm
Energy, a.u.	-5642.78586202				-5642.78586431
E _{rel} , kcal/mol					
d(Fe=O), Å	1.63225				1.63220
∠(O-Fe=O)	107.805				107.792
∠(O-Fe-O)	144.389				144.410
<S ² >	6.0583				6.0583
q _s (Fe)	3.159				3.159
q _s (O)	0.533				0.533
E(Fe1s), a.u.	-256.196426				-256.196439
E(O1s), a.u.	-19.175179				-19.175195
E(Fe1s), eV.	-6971,459845				-6971,460199

E(O1s), eV	-521,7831978				-521,7836332
E _{rel} (Fe1s), eV.	0				-0,000354
E _{rel} (O1s), eV	0				-0,0004354

$$E_{\text{ads}} = E(\text{NoSymm}+\text{CH}_4) - (E(\text{NoSymm}) + E(\text{CH}_4)) = -5683.32060760 - (-5642.78586431 - 40.5339575449) = -0.000785745 \text{ (a.u.)} = -0.493062515 \text{ (kcal/mol)}$$

Table 4. Characteristics of adsorbed system, reactants, transition state and products for $\text{O}=\text{Fe}(\text{OGa}(\text{OH})_2)+\text{CH}_4$

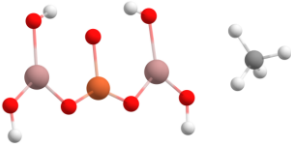
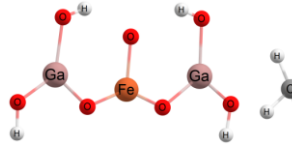
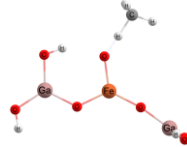
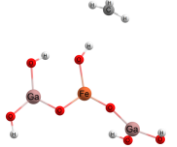
Structure	NoSymm+CH ₄	Reactants	TS	Products
				
Energy, a.u.	-5683.32060760	-5683.32060472	-5683.29165928	-5683.30658086
E _{rel} , kcal/mol	0	0	18,17	8,8
d(Fe=O), Å	1.63237	1.63237	1.76131	1.82619
∠(O-Fe=O)	107.806	107.806	108.452 124.864	109.631 124.947
∠(O-Fe-O)	144.368	144.374	126.683	125.422
∠(Fe-O-H)	87.121	87.051	137.973	128.488
∠(Fe-O-C)	76.586	76.505	138.786	134.257
<S ² >	6.0583	6.0583	6.7086	7.0056
q _s (Fe)	3.158	3.158	3.980	4.118
q _s (O)	0.533	0.533	-0.046	0.276
q _s (H)	0	0	-0.002	-0.038
q _s (C)	0.001	0.001	-0.484	-1.071
E(Fe1s), a.u.	-256.195370	-256.195370	-256.177040	-256.176870
E(O1s), a.u.	-19.174100	-19.174100	-19.149210	-19.138290
E(Fe1s), eV.	-6971,43111	-6971,43111	-6970,932325	-6970,927699
E(O1s), eV	-521,7538367	-521,7538367	-521,0765453	-520,779397
E _{rel} (Fe1s), eV.	0	0	0,498785	0,503411
E _{rel} (O1s), eV	0	0	0,6772914	0,9744397

Table 5. The different states of $\text{O}=\text{Fe}(\text{Al}(\text{OH})_2)_2(\mu\text{-O})_4(\text{Si}(\text{OH})_2)_2$ model in C_{2v} point group: energy, geometrical parameters, spin densities, <S²> and energy of 1s-orbital of Fe and O from group [FeO]²⁺.

Symmetry	⁵ A ₁	⁵ A ₂	⁵ B ₁	⁵ B ₂	NoSymm
Energy, a.u.	-3311.54420701	-3311.50143231	-3311.54568887	-3311.54706312	-3311.55915096
E _{rel} , kcal/mol	0	26,84153061	-0,929881228	-1,792236158	-9,377470593
d(Fe=O), Å	1.60328	1.70177	1.75535	1.75709	1.60708
∠(O-Fe=O)	118.090	115.301	119.950	119.976	108.176 98.418
∠(O-Fe-O)	123.820 123.820	129.397 129.397	120.101 120.101	120.047 120.047	134.909 107.991
<S ² >	6.1779	6.1013	6.7496	6.7531	6.0774
q _s (Fe)	3.303	2.883	4.012	4.044	3.148
q _s (O)	0.258	1.246	-0.552	-0.566	0.565

E(Fe1s), a.u.	-256.215664	-256.170853	-256.220635	-256.220401	-256.211729
E(O1s), a.u.	-19.201990	-19.141748	-19.195135	-19.195061	-19.193293
E(Fe1s), eV.	-6971,983337	-6970,763968	-6972,118605	-6972,112238	-6971,876261
E(O1s), eV	-522,5127622	-520,8734939	-522,3262282	-522,3242145	-522,2761048
E _{rel} (Fe1s), eV.	0	1,219369	-0,135268	-0,128901	0,107076
E _{rel} (O1s), eV	0	1,6392683	0,186534	0,1885477	0,2366574

$$E_{\text{ads}} = E(\text{NoSymm}+\text{CH}_4) - (E(\text{NoSymm}) + E(\text{CH}_4)) = -3352.09365313 - (-3311.55915096 - 40.5339575449) = -0.000544625 \text{ (a.u.)} = -0.341757424 \text{ (kcal/mol)}$$

Table 6. Characteristics of adsorbed system, reactants, transition state and products for $O=\text{Fe}(\text{Al}(\text{OH})_2)_2(\mu\text{-O})_4(\text{Si}(\text{OH})_2)_2 + \text{CH}_4$

Structure	NoSymm+CH ₄	Reactants	TS	Products
Energy, a.u.	-3352.09365313	-3352.10086859	-3352.09823616	-3352.11650537
E _{rel} , kcal/mol	4,527769697	0	1,651874833	-9,812227999
d(Fe=O), Å	1.60792	1.75673	1.74692	1.77334
∠(O-Fe=O)	98.418 108.190	124.649 120.188	113.371 125.102	119.439 118.639
∠(O-Fe-O)	108.022 134.952	115.642 125.048	115.243 125.110	114.747 125.103
∠(Fe-O-H)	178.928	114.315	123.484	135.477
∠(Fe-O-C)	179.189	104.701	120.736	134.938
<S ² >	6.0778	6.7541	6.7362	6.9929
q _s (Fe)	3.143	4.046	4.017	4.093
q _s (O)	0.568	-0.552	-0.216	0.381
q _s (H)	0.002	-0.006	-0.006	-0.032
q _s (C)	-0.002	-0.007	-0.291	-1.053
E(Fe1s), a.u.	-256.212310	-256.220820	-256.204890	-256.200640
E(O1s), a.u.	-19.193480	-19.194690	-19.174420	-19.147700
E(Fe1s), eV.	-6971,89207	-6972,123639	-6971,690162	-6971,574514
E(O1s), eV	-522,2811933	-522,3141191	-521,7625443	-521,0354561
E _{rel} (Fe1s), eV.	0	-0,231569	0,201908	0,317556
E _{rel} (O1s), eV	0	-0,0329258	0,518649	1,2457372

$$E_{\text{ads}} = E(\text{NoSymm}+\text{CH}_4) - (E(\text{NoSymm}) + E(\text{CH}_4)) = -6716.72352955 - (-6676.19577210 - 40.5339575449) = 0.006200095 \text{ (a.u.)} = 3.89061845 \text{ (kcal/mol)}$$

Table 7. The different states of $O=\text{Fe}(\text{Ga}(\text{OH})_2)_2(\mu\text{-O})_4(\text{Si}(\text{OH})_2)_2$ model in C_{2v} point group: energy, geometrical parameters, spin densities, <S²> and energy of 1s-orbital of Fe and O from group [FeO]²⁺.

Symmetry	⁵ A ₁	⁵ A ₂	⁵ B ₁	⁵ B ₂	NoSymm
Energy, a.u.	-6676.17718700				-6676.19577210
E _{rel} , kcal/mol					
d(Fe=O), Å	1.60352				1.60533
∠(O-Fe=O)	117.147				111.254 100.479
∠(O-Fe-O)	125.706 125.706				135.000 113.227
<S ² >	6.1760				6.1103
q _s (Fe)	3.320				3.241
q _s (O)	0.256				0.430

E(Fe1s), a.u.	-256.210917				-256.209420
E(O1s), a.u.	-19.196999				-19.191630
E(Fe1s), eV.	-6971,854165				-6971,81343
E(O1s), eV	-522,3769502				-522,2308523
E _{rel} (Fe1s), eV.	0				0,040735
E _{rel} (O1s), eV	0				0,1460979

Symmetry	NoSymm
Energy, a.u.	-4785.17740446
d(Fe=O), Å	1.60555
∠(O-Fe=O)	97.371 152.774
∠(O-Fe-O)	166.245 100.728
<S ² >	6.0603
q _s (Fe)	3.102
q _s (O)	0.736
E(Fe1s), a.u.	-256.218220
E(O1s), a.u.	-19.204390
E(Fe1s), eV.	-6972,05289
E(O1s), eV	-522,5780696

$$E_{\text{ads}} = E(\text{NoSymm}+\text{CH}_4) - (E(\text{NoSymm}) + E(\text{CH}_4)) = -4825.71243280 - (-4785.17740446 - 40.5339575449) = -0.001070795 \text{ (a.u.)} = -0.671934098 \text{ (kcal/mol)}$$

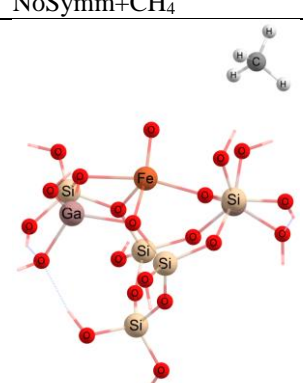
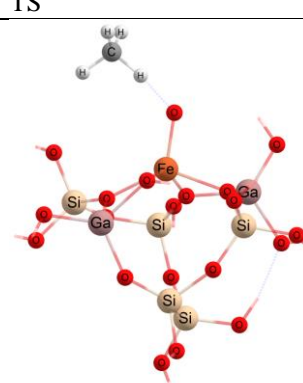
Table 8. Characteristics of adsorbed system, reactants, transition state and products for 6-ring model ZSM-5 (FeAl2Si5H12O21) + CH₄

Structure	NoSymm+CH ₄	Reactants	TS	Products
Energy, a.u.	-4825.71243280	-4825.73380372	-4825.72808972	-4825.74702002
E _{rel} , kcal/mol	13,41045532	0	3,585589283	-8,293353805
d(Fe=O), Å	1.60619	1.60277	1.73064	1.78574
∠(O-Fe=O)	96.317 152.860	128.369 101.322	103.463 124.631	108.609 102.747
∠(O-Fe-O)	165.889 100.809	145.059 131.852	146.403 131.861	154.291 130.300
∠(Fe-O-H)	120.269	124.508	132.508	131.762
∠(Fe-O-C)	120.269	114.000	129.126	130.559
<S ² >	6.0607	6.1214	6.6583	6.9896
q _s (Fe)	3.099	3.249	3.970	4.158
q _s (O)	0.733	0.425	-0.167	0.413
q _s (H)	0.02	0	-0.008	-0.031
q _s (C)	0.000	0	-0.205	-1.069
E(Fe1s), a.u.	-256.218550	-256.216300	-256.210160	-256.203930
E(O1s), a.u.	-19.204070	-19.202180	-19.181200	-19.147940
E(Fe1s), eV.	-6972,06187	-6972,000644	-6971,833566	-6971,664039
E(O1s), eV	-522,5693619	-522,5179324	-521,9470375	-521,0419868
E _{rel} (Fe1s), eV.	0	0,061226	0,228304	0,397831
E _{rel} (O1s), eV	0	0,0514295	0,6223244	1,5273751

Symmetry	NoSymm
Energy, a.u.	-8149.80635589
d(Fe=O), Å	1.60657
∠(O-Fe=O)	95.837 97.359
∠(O-Fe-O)	166.120 101.501
<S ² >	6.0595
q _s (Fe)	3.106
q _s (O)	0.734
E(Fe1s), a.u.	-256.214850
E(O1s), a.u.	-19.200190
E(Fe1s), eV.	-6971,961187
E(O1s), eV	-522,4637817

$$E_{\text{ads}} = E(\text{NoSymm}+\text{CH}_4) - (E(\text{NoSymm}) + E(\text{CH}_4)) = -8190.34175660 - (-8149.80635589 - 40.5339575449) = -0,001443165 \text{ (a.u.)} = -0,90559981 \text{ (kcal/mol)}$$

Table 9. Characteristics of adsorbed system, reactants, transition state and products for 6-ring model ZSM-5 (FeGa2Si5H12O21) +CH₄

Structure	NoSymm+CH ₄	Reactants	TS	Products
				
Energy, a.u.	-8190.34175660	-8190.36227521	-8190.35592933	-8190.37478040
E _{rel} , kcal/mol	12,8756227	0	3,982099986	-7,847125525
d(Fe=O), Å	1.60713	1.60357	1.74013	1.79239
∠(O-Fe=O)	95.912 153.136	123.410 104.612	123.460 110.147	95.964 101.896
∠(O-Fe-O)	165.966 101.544	154.200 134.210	147.796 133.408	146.977 134.231
∠(Fe-O-H)	122.342	147.660	130.192	128.152
∠(Fe-O-C)	117.509	142.971	126.540	122.516
<S ² >	6.0595		6.6823	
q _s (Fe)	3.104	3.273	4.007	4.183
q _s (O)	0.733	0.399	-0.185	0.4
q _s (H)	0.001	0.002	-0.005	-0.017
q _s (C)	0.000	-0.002	-0.220	-1.082
E(Fe1s), a.u.	-256.214910		-256.205220	
E(O1s), a.u.	-19.199710		-19.174530	
E(Fe1s), eV.	-6971,96282		-6971,699142	
E(O1s), eV	-522,4507203		-521,7655376	
E _{rel} (Fe1s), eV.	0		0,263678	
E _{rel} (O1s), eV	0		0,6851827	

